# Enhancing Forward Progress of Transient Systems by Optimising Capacitor Size

Jie Zhan, Alex S. Weddell, *Member, IEEE,* and Geoff V. Merrett, *Member, IEEE*

***Abstract*—Energy-harvesting batteryless devices are promising for a sustainable IoT. Forward progress in such devices is maintained by transient computing, where volatile computing state is saved into and restored from nonvolatile memory before and after power failures. In transient computing systems, only a minimised energy storage, e.g. a decoupling capacitor, is used to ensure the most energy-expensive atomic operation. To evaluate forward progress of such systems in deployment requires considerations on energy source variability and understanding of transient computing. In this paper, we present a model framework of energy-harvesting transient computing devices, as well as a theoretical transient computing load model, to estimate forward progress under variable energy source conditions. Using this model, we show that energy storage capacity beyond the minimum improves forward progress by reducing state-saving and -restoring overheads. We propose a process of identifying the proper energy storage capacity to balance forward progress, dimensions, and recharging time. Following this process, properly sizing energy storage gains up to 35.0% mean forward progress improvement through simulation with one-year indoor and outdoor light energy source traces. With experimental validation based on an MSP430FR6989 microcontroller, using a suggested 43 µF capacitor rather than an on-board 10 µF one improves forward progress by up to 30.4% given various current income.**

***Index Terms*—intermittent computing, transient computing, energy harvesting, energy storage, forward progress, batteryless, wireless sensor networks, internet of things.**

## I. Introduction

To establish a ubiquitous Internet of Things (IoT), tens of billions of devices are to be installed, and possibly at hard-to-reach locations [1]–[4]. Using non-rechargeable batteries constrains the lifespan of these devices and brings impractical battery replacement work. Enabling IoT devices to harvest ambient energy becomes a solution to circumvent the limited battery lifespan.

Environmentally harvested power is intrinsically variable and intermittent [5]. Traditionally, large energy storage, in forms of rechargeable batteries or supercapacitors, is adopted to buffer the variable harvested power and provide reliable power [6]–[11]. Unfortunately, such types of energy storage still limit device lifespan, increase cost and size, and raise pollution concerns, while directly using an energy-harvesting supply without energy buffering hinders execution by frequent power failures.

~~To remove large energy storage while maintain execution despite frequent power failures, recent research has developed *transient computing* (also known as *intermittent computing*)~~ which saves and restores system volatile computing state (e.g. CPU register data, RAM data) through nonvolatile memory (NVM) [12]–[17]. During active periods, the system volatile state is saved into NVM either at pre-installed points (*static*) or just before the power supply fails (*reactive*) [18]. The volatile state is lost when the supply voltage drops below the minimum operating threshold, while the saved state in NVM is retained. The saved state is restored from NVM when the supply voltage recovers to a restore threshold, and then the execution continues from the last saved point. Therefore, forward execution is preserved without large energy storage despite frequent supply failures. In transient computing, forward progress denotes the effective program progress, as opposed to re-executed progress, lost progress, and the progress of state-saving and -restoring operations [19], [20]. The amount of forward progress directly determines application performance (e.g. program iteration rate or task completion time).

With the goal of minimising device dimensions and recharging time, previous designs in transient computing typically adopt only a minimum amount of energy storage, e.g. a decoupling capacitor, which is just enough for the most energy-expensive atomic operation[1] [13], [14], [...]–[25]. However, in exploration we found that, a device with only minimum energy storage has to frequently wake up, execute shortly, and halt, consuming much energy in saving and restoring system states when power production is less than power consumption (which is common in energy-harvesting devices).

In this paper, we present a framework of energy-harvesting transient computing (EHTC) devices, as well as a theoretical model of reactive transient computing to estimate forward progress. Taking advantage of the theoretical model, we explore the effect of energy storage capacity on forward progress with respect to supply current and volatile state size. We found that provisioning more energy storage prolongs the operating cycles, and hence improves forward progress by reducing the state-saving and -restoring overheads; however a larger capacitor also increases leakage current, occupies more volume, and requires longer recharging time. We propose a process of identifying the proper energy storage size for deploying EHTC devices, which improves forward progress and balances dimensions and recharging time. We integrate the reactive transient computing model in a photovoltaic-based (PV-based) EHTC device framework. We demonstrate the sizing process with the framework given various real-world indoor and outdoor light source datasets.

~~In brief~~, the contributions of this paper are:

Software of this work will be open-source upon acceptance of this paper.

[1]Atomic operations in transient computing denote operations that should be completed in one continuous period. If an atomic operation is interrupted by a power failure, it should be re-executed rather than resumed. One example of atomic operations is saving and restoring volatile state.

- A theoretical model of reactive transient computing to estimate forward progress.
- An exploration of the energy storage sizing effect on forward progress with respect to supply current and volatile state size.
- A process of determining the energy storage size in deploying EHTC devices, which trades off forward progress, capacitor dimensions, and recharging time.
- A demonstration of the sizing process with the reactive transient computing model integrated in a PV-based EHTC device framework, where results show that a reasonbly energy storage capacity, rather than a minimum one, can improve 5.5-28.7% mean forward progress, while balance capacitor volume and recharging delay, given four different one-year real-world energy source datasets.
- Experimental validation of the theoretical model, which shows high accuracy with 0.5% mean absolute percentage error (MAPE), and a reasonbly sized 43 µF capacitor improves forward progress by up to 55.2% and 30.4% compared to a theoretical minimum 6.2 µF one and an on-board 10 µF one across various levels of supply current.

The rest of this paper is organized as follows. Background and related work on transient computing and its modelling approaches are provided in Section II. Our modelling method is illustrated in Section III. The sizing process is presented in Section IV. Model and simulation setup is explained in Section V. Design exploration and demonstration of the sizing process is presented in Section VI. The theoretical model is experimentally validated in Section VII. Finally, Section VIII concludes this paper.

## II. Background and Related Work

### A. Transient Computing

The goal of transient computing is to enable devices to maintain progress despite frequent power failures, such that the devices can operate even directly powered by energy harvesters without large energy storage. The basic mechanism is to back up volatile computing state (lost if the supply fails) as nonvolatile state (preserved if the supply fails) during active periods; when the supply recovers, the lost volatile state is restored from the saved nonvolatile state to resume execution. In principles, approaches in transient computing can be classified as *static* and *reactive*.

*1) Static Transient Computing:* Static approaches save volatile state into NVM at compile-time pre-installed points in a program, either by inserting checkpoints or decomposing a program into atomic tasks. After power failures, the execution resumes from the last saved checkpoint or the last task boundary. Advantages in static approaches include eliminating additional hardware and ensuring operation atomicity. However, the rollback of progress intrinsically causes code re-execution, which introduces issues on memory consistency and wastes energy on both lost and re-executed progress. Also, if the code between two successive checkpoints or task boundaries exceeds the amount that the energy storage can guarantee, the progress may never proceed due to insufficient power income.

*2) Reactive Transient Computing:* In contrast to static approaches, reactive approaches save volatile state in NVM when supply is about to fail by monitoring supply voltage. Specifically, reactive transient computing saves volatile state and enters a low-power mode (execution halted) if supply voltage falls below a save threshold. This save threshold should be set high enough to save volatile state before power fails. By entering the low-power mode, reactive approaches avoids re-execution, and hence, typically make more forward progress than static approaches. In a comparison between static [26] and reactive [13] approaches, the reactive approach achieves a 2.5× mean speedup in computational workloads [27]. Therefore, reactive transient computing is the focus in this work.

### B. Related Work on Modelling Transient Computing

A few models about transient computing have been proposed to explore design space. Su et al. [28] provide a model to explore the impact of sizing energy harvester and energy storage on a dual-channel solar-powered nonvolatile sensor node, but their exploring range of supercapacitors spans from 10F to $10^4$F, which is significantly larger than a typical scale of energy storage (µF to mF scale) in transient computing. EH model [29], [30] explores forward progress with different parameter settings in transient computing, but the model only considers a single active period without considering inactive periods that scale down the effective forward progress, and hence, the model cannot predict the effective forward progress. Jackson et al. [31] also present a modelling approach to explore energy storage effect, where they suggest that novel batteries are preferable in order to offer reliable task completion and to improve energy utilization. However, they do not provide guidance on how to design energy storage, and their model lacks the state-saving and -restoring mechanism in transient computing.

We provide a modelling approach to estimate forward progress of an EHTC device in real-world deployment, considering energy source conditions as well as the forward progressing behaviours transient computing. This model can be used to explore the effect of energy harvester and energy storage sizing on forward progress. Further, we provide a process of sizing energy storage in transient systems.

## III. Modelling Transient Computing Devices

The goal of this model is to estimate forward progress of EHTC devices in real-world deployment. In this section, we introduce the framework of this model for general transient computing devices, and then present a load model of reactive transient computing for estimating forward progress based on its theoretical behaviours. In this model, without being restricted to a specific workload, **we describe forward progress as the ratio of the effective execution time to the total time**, based on an assumption that application progress is linear to execution time. ~~Following this section, we use this model to explore~~ the effect of energy storage capacity and energy harvester size on forward progress.

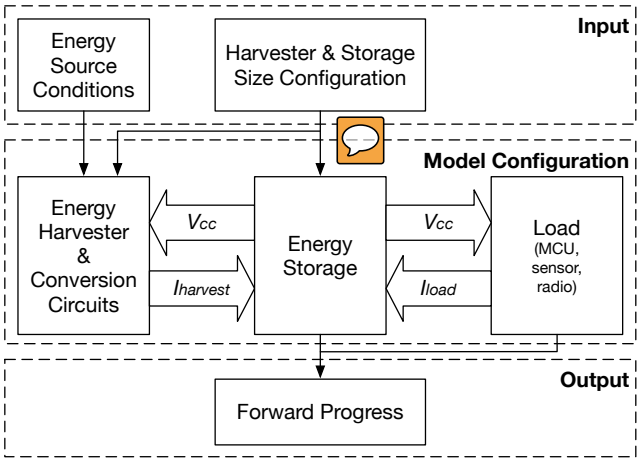


Fig. 1. Model framework of EHTC devices for estimating forward progress in real-world deployment.

TABLE I
MODEL PARAMETERS OF REACTIVE TRANSIENT COMPUTING

| | |
|---|---|
| **Input Parameters** | |
| $I_{harv}$ | Energy harvester current supply |
| $C$ | Energy storage capacitance |
| **Configuration Parameters** | |
| $I_{exe}$ | Execution current consumption |
| $I_{sleep}$ | Sleep current consumption |
| $I_r$ | Restore current consumption |
| $I_s$ | Save current consumption |
| $I_{leak}$ | Leakage current consumption |
| $V_r$ | Restore voltage threshold |
| $V_s$ | Save voltage threshold |
| $T_r$ | Restore time overhead |
| $T_s$ | Save time overhead |
| **Output Parameter** | |
| $\alpha_{exe}$ | Effective execution time ratio (forward progress) |

### A. Model Framework

The model framework is shown in Fig. 1. The model is driven by energy source conditions as a function of time. The configuration of this model includes three modules, *Energy Harvester and Conversion Circuits*, *Energy Storage*, and *Load*, which can be individually specified to represent the target platform. The three modules communicate by their voltage and current flows. This model outputs the time distribution of estimated forward progress over the test period of energy source input.

*1) Model Inputs:* This model takes two inputs, a) energy source conditions, and b) the size configuration of energy harvester and energy storage. The unit of energy source conditions should be consistent with the unit of the *Energy Harvester and Conversion Circuits* module. In this model, we assume that the energy source is equally distributed in the deployed space, such that increasing the size of energy harvester leads to more exposure to ambient energy, and vice versa. Note that the size configuration of energy harvester configures actual dimensions, while the one of energy storage configures capacity.

*2) Model Configuration:* Due to the variety of each module, the model configuration depends on the techniques implemented for each module.

*Energy Harvester and Conversion Circuits.* The energy harvester model transduces energy source conditions into electrical power. Typically, the power harvested from the energy harvester should be conditioned to provide a suitable voltage for charging the energy storage and supplying the load efficiently. For example, solar power from a solar panel is typically paired with a maximum power point tracking circuit to effectively extract solar power. The model should be configured for the specific energy harvester and the corresponding conversion circuits. However, in transient computing, such conversion circuits may be removed to increase power efficiency, using only a diode to prevent current backflow. We model energy harvester and conversion circuits together as a module because they are usually coupled and integrated.

*Energy Storage.* Energy storage in transient computing devices is usually in the form of a μF-scale capacitor. The energy storage provides the minimum length of an execution period, which is minimised to just ensure the most energy expensive operation in recent literature.

*Load.* The load module includes all the power consumers in a transient computing device, such as a microcontroller, sensors, and a radio. Techniques in transient computing dominate how the load consumes power and makes forward progress. As mentioned in Section I and Section II, transient computing approaches can be classified as *static* and *reactive*. Different approaches require different models for estimating forward progress. However, to model transient computing is still a challenge due to lack of understanding and abstraction of its behaviours.

### B. Forward Progress of Reactive Transient Computing

We present a theoretical method to understand and model the forward progress in reactive transient computing given a constant current supply. This model includes *Energy Storage* and *Load* modules in the model framework. The parameters of this model are listed in TABLE I. The model inputs, i.e. $I_{harv}$ and $C$, are related to the size configuration of energy harvester and energy storage respectively. The model output is $\alpha_{exe}$, the average forward progress when a constant current supply is applied for a period of time, which is long enough to omit an individual uncompleted operating cycle and recharging time. In the model we assume that all the parameters maintains constant at their average values during the time period.

Because supply current $I_{harv}$ and leakage current $I_{leak}$ constantly exist (though could be zero), we use $I_{in}$ to denote usable current income for equation simplicity:

$$I_{in} = I_{harv} - I_{leak} \tag{1}$$

The capacitor leakage effect is discussed at the end of in this section.

*1) Operating Modes of Transient Computing Devices:* The computing behaviours of reactive transient computing devices can be classified as three operating modes given a spectrum of supply current. As shown in Fig. 2, an empirical experiment

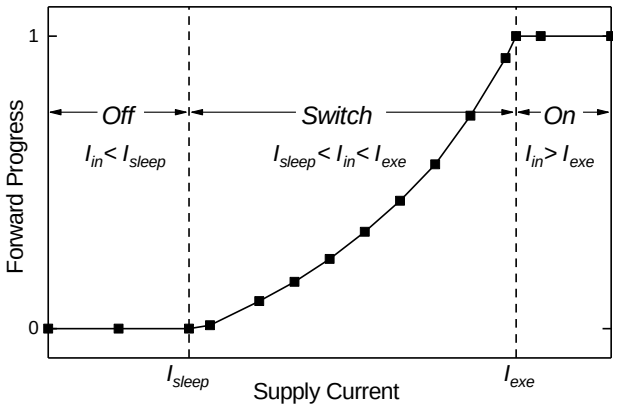


Fig. 2. Operating modes of reactive transient computing devices according to supply current and forward progress.

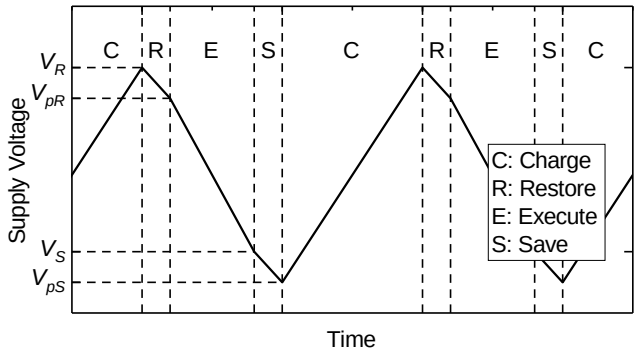


Fig. 3. Operating cycles in the Switch mode.

demonstrates the three operating modes. These three modes are divided by the relationship between the system current income and current consumption. We denote the three modes by *Off*, *Switch*, and *On*.

*Off mode*: When $I_{in} < I_{sleep}$, the device cannot wake up. The supply voltage $V_{cc}$ cannot be charged up to the restore threshold $V_r$ to start execution, so the device stays inactive. The sleep current $I_{sleep}$ denotes the current consumption when the device waits for supply voltage to recover above the restore threshold, and hence, includes the consumption of voltage monitoring circuits.

*Switch mode*: When $I_{sleep} < I_{in} < I_{exe}$, the device executes transiently. $V_{cc}$ can be charged up to $V_r$ and the device starts execution. However, the energy in energy storage is then consumed by the load as $I_{in} < I_{exe}$, causing $V_{cc}$ to drop below the save threshold $V_r$, where the device saves its state and sleeps. The device sleeps until $V_{cc}$ charges to $V_r$ again and then resumes the execution. In this mode, $V_{cc}$ oscillates approximately between $V_r$ and $V_s$, 'switching' on and off the execution. In general, higher $I_{harv}$ leads to more forward progress in this mode, but the exact relationship between $I_{harv}$ and forward progress requires further analysis.

*On mode*: When $I_{in} > I_{exe}$, the device execute constantly as the supply voltage $V_{cc}$ never fails. The excessive power either dissipates through circuits or overcharges $V_{cc}$. An overcharged $V_{cc}$ may affect harvesting efficiency (due to poor impedance matching) and reduce $I_{harv}$, such that current income and consumption are in equilibrium.

*2) Formulating Forward Progress:* We aim to calculate how much forward progress is made in relation to energy storage capacity and current income through a theoretical analysis. In the following analysis, we focus on the Switch mode ($I_{sleep} < I_{in} < I_{exe}$), as the forward progress of the On mode and the Off mode is straightforward (i.e. 1 in the On mode and 0 in the Off mode).

In the Switch mode, as shown in Fig. 3, the device goes through four intervals in turn, i.e. charging, restoring, executing, and saving, with current consumption of $I_{sleep}$, $I_r$, $I_{exe}$, and $I_s$ in each interval respectively.

Let $V_{pr}$ (post-restore) and $V_{ps}$ (post-save) denote the voltage after restoring and saving operations. $V_{pr}$ and $V_{ps}$ can be calculated as:

$$\begin{aligned} V_{pr} &= V_r + \frac{T_r(I_{in} - I_r)}{C} \\ V_{ps} &= V_s + \frac{T_s(I_{in} - I_s)}{C} \end{aligned} \tag{3}$$

Then, the time spent on useful execution $T_{exe}$ in one operating cycle can be expressed as:

$$\begin{aligned} T_{exe} &= \frac{C(V_{pr} - V_s)}{I_{exe} - I_{in}} \\ &= \frac{C(V_r - V_s) + T_r(I_{in} - I_r)}{I_{exe} - I_{in}} \end{aligned} \tag{4}$$

In Equation (4), the first term in the numerator represents the amount of energy in the storage capacitor for restoring and executing. The second term in the numerator represents the restoring cost. The denominator is the current consumption for execution.

Also, the charging interval can be described as:

$$\begin{aligned} T_{charge} &= \frac{C(V_r - V_{ps})}{I_{in} - I_{sleep}} \\ &= \frac{C(V_r - V_s) - T_s(I_{in} - I_s)}{I_{in} - I_{sleep}} \end{aligned} \tag{5}$$

Then, with Equation (4) and (5), the period of an operating cycle is:

$$\begin{aligned} T_{period} = \; & T_{charge} + T_r + T_{exe} + T_s \\ = \; & \frac{C(V_r - V_s) + T_s(I_{in} - I_s)}{I_{in} - I_{sleep}} + \\ & \frac{C(V_r - V_s) + T_r(I_{exe} - I_r)}{I_{exe} - I_{in}} \end{aligned} \tag{6}$$

Finally, with $T_{exe}$ and $T_{period}$ calculated in Equation (4) and (6), we obtain the percentage of time spent on effective execution (forward progress) in the Switch mode:

$$\alpha_{exe} = \frac{T_{exe}}{T_{period}}, \quad I_{sleep} < I_{in} < I_{exe} \tag{7}$$

Higher $\alpha_{exe}$ leads to more time spent on forward progress. As $d\alpha_{exe}/dI_{in}$ is positive[2], higher harvested current $I_{harv}$ leads to more forward progress. To find out the energy storage effect on $\alpha_{exe}$, we need to analyze $d\alpha_{exe}/dC$. Here, if we

[2]Calculation breakdowns of differential analysis is attached in Appendix.

assume the leakage current maintains constant when storage capacity increases, $\alpha_{exe}$ keeps increasing with $C$ to approach $(I_{in} - I_{sleep})/(I_{exe} - I_{sleep})$, which is an ideal case where restore and save overheads are zero. However, in an electrolyte capacitor, the leakage current typically increases with storage capacity $C$ in the following relationship:

$$I_{leak} = kCV_{cc} \tag{8}$$

where $k$ is a constant normally in a range from 0.01 to 0.03 ($\frac{A}{F \cdot V}$). Therefore, referring to Equation (1), $dI_{in}/dC$ is $-kV_{cc}$, which is negative. Hence, considering capacitor leakage increases with capacitance, there is an optimal capacity that leads to the maximum forward progress $\alpha_{exe}$.

To include the Off and On modes (to recall, Off: $I_{in} < I_{sleep}$, On: $I_{in} > I_{exe}$), the forward progress given all supply levels is described as:

$$\alpha_{exe} = \begin{cases} 0 & , \quad I_{in} < I_{sleep} \\ \dfrac{T_{exe}}{T_{period}} & , \quad I_{sleep} < I_{in} < I_{exe} \\ 1 & , \quad I_{in} > I_{exe} \end{cases} \tag{9}$$

where $T_{exe}$ and $T_{period}$ are calculated by Equation (4) and (6) respectively.

## IV. Process of Sizing Energy Storage

Leveraging our model, we propose a process of identifying the optimal capacitor size that improves forward progress and balances the side effects, i.e. increased dimensions and recharging time. The process follows the steps below.

**S1- Determine design specifications**: Derive specifications according to a target application, such as minimum forward progress, minimum energy storage capacity, maximum capacitor dimensions, and maximum recharging time under certain energy source conditions.

**S2- Configure model**: Configure the model as explained in Section III according to the target platform and application, and collect energy source conditions of the environment where the device is deployed (demonstrated in Section V).

**S3- Size Energy Harvester** With the configured model, run tests with the minimum capacitance, and find the energy harvester size to ensure the minimum forward progress under the given energy source conditions.

**S4- Optimise capacitor size**: Generate the relationship between forward progress and capacitance. Evaluate the optimal capacitance by balancing the side effects of capacitor volume and recharging time with forward progress in a cost function. Here, we suggest a cost function as:

$$f = \frac{\alpha_{exe}}{k_1} - (\frac{v_{cap}}{k_2})^2 - (\frac{T_{recharge}}{k_3})^2 \tag{10}$$

where $v_{cap}$ represents capacitor volume and $T_{recharge}$ represents recharging time. $k_1$, $k_2$, and $k_3$ are linear scalers, which are empirically determined according to design specifications. The negative side effects are calculated in quadratic forms so as to punish high values heavier. We only consider the above three factors in this paper to size energy storage, but other factors (e.g. dimensions of energy harvesters) can be certainly included to consider a broader scenario.

We demonstrate this process to optimise the capacitor size in the next two sections (Section V and Section VI). We do not determine design specifications with specific numbers as we do not target a specific application, but we discuss these design specifications.

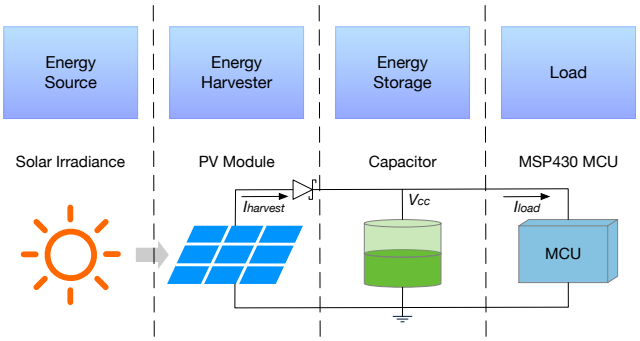


Fig. 4. Model configuration of a PV-based EHTC device.

## V. Model Configuration

This section explains how this model framework is configured for design exploration in a PV-based EHTC device. Energy harvester and energy storage are modelled by existing models of PV cells and capacitors. We use a converter-less architecture where there is only a diode at the energy harvester output for preventing current backflow. The load is modelled by the forward progress formulation in Section III-B, with parameters profiled on a TI MSP430FR6989 MCU. A diagram of the configured model is shown in Fig. 4.

### A. Energy Source and Energy Harvester

We import NREL outdoor solar irradiance data [32] and EnHANTs indoor irradiance data [33] as the energy source conditions input. To convert irradiance to energy harvester power output, we adopt a datasheet-based PV cell model [34] developed recently. This model takes the parameters available in common PV cell datasheets, so it is easily reconfigured to suit different PV cells. According to this model, the output current $I_o$ of a PV cell can be described as:

$$I_o = \frac{G}{G_{ref}} I_{sc}(1 - (1 - \frac{I_{mpp}}{I_{sc}})^{\frac{V_o - V_{oc}}{V_{mpp} - V_{oc}}}) \tag{11}$$

where $V_o$ is the output voltage of the PV cell, $G$ is the ambient irradiance, $G_{ref}$ is the reference irradiance (normally $1000W/m^2$), and $I_{sc}$, $V_{oc}$, $I_{mpp}$, $V_{mpp}$ are respectively short-circuit current, open-circuit voltage, and the current and voltage at maximum power point (MPP) given the reference irradiance. $V_o$ and $G$ are dynamic at run time, while other parameters in this model are constant.

A PV panel is an array of PV cells, which amplifies voltage and current output by connecting PV cells in series or parallel. In a PV panel, the open-circuit voltage is proportional to the number of cells in series, and the short-circuit current is

TABLE II
PV CELL MODEL PROPERTIES

| Parameter | Value |
|---|---|
| Open-Circuit Voltage | 0.89 V/cell |
| Short-Circuit Current | 14.8 mA/cm$^2$ |
| MPP Voltage | 0.65 V/cell |
| MPP Current | 12.1 mA/cm$^2$ |

proportional to the area of each cell and the number of cells in parallel. We refer to a commercial solar cell [35] for PV cell properties as shown in TABLE II. We set four cells in series (with $V_{oc}$ = 3.56V) to match the operating voltage of the MCU (maximum 3.6V), and model energy harvester sizing by scaling the cell area. A Schottky diode is connected to the energy harvester output in order to prevent current backflow.

### B. Energy Storage

The energy storage is represented as an ideal capacitor with capacitance-related current leakage. The terminal voltage of this buffering capacitor is directly applied to the load, so this capacitor is modelled as:

$$C\frac{dV_{cc}}{dt} = I_{harv} - I_{load} - I_{leak} \tag{12}$$

where $I_{load}$ is the current consumption of the load. The leakage current $I_{leak}$ in electrolytic capacitors demonstrates complex physical phenomenon. In the model exploration, we refer to the datasheet of a commercial aluminium capacitor [36] to represent empirical $I_{leak}$ in relation to capacitance $C$:

$$I_{leak} = max\{0.03CV_{rated}, \quad 4 \times 10^{-6}\} \quad (A) \tag{13}$$

where $V_{rated}$ is the capacitor rated voltage. $V_{rated}$ is chosen to be 10 V so as to operate the load (typically $<$ 4.0 V) around 25-40 % of the rated voltage for low leakage design [37].

### C. Load

We implemented a reactive transient computing approach [14] on a TI MSP430FR6989 microcontroller. We profiled the model parameters by setting the MCU clock frequency at 8 MHz, running Dijkstra path finding algorithm with 1696B RAM usage in total. The supply voltage monitoring circuits use the MCU internal comparator and an external 3 MΩ voltage divider. The restore and save voltage thresholds are set as $V_r$ = 2.4 V and $V_s$ = 2.1 V. The MCU shutdown voltage is $V_{off}$ = 1.8 V.

The profiled parameters are shown in TABLE III. We measured the current consumption with a range of supply voltage. In experimental measurements, the variation of $I_{sleep}$ between $V_{off}$ and $V_r$ is 2%, and the variation of $I_{exe}$ between $V_s$ and 3.3 V is 1.5%. $I_{exe}$ also has a run-time variation of -2.4% to +2.8% with constant supply voltage due to a variable memory access rate. We omit such negligible variations and use the mean of $I_{exe}$ and $I_{sleep}$ in the model. $I_r$ and $I_s$ are measured at $V_r$ and $V_s$ respectively. Given the voltage thresholds and the current consumption, the minimum energy storage to guarantee save and restore operations is 6.2 µF.

TABLE III
PROFILED MCU PARAMETERS

| Parameter | Value |
|---|---|
| $I_{exe}$ | 887 µA |
| $I_{sleep}$ | 26 µA |
| $I_r$ | 971 µA |
| $I_s$ | 811 µA |
| $T_r$ | 1.903 ms |
| $T_s$ | 1.880 ms |

Although we define the parameters in our model, however, these parameters can be tuned to explore different load characteristics. For example, $T_r$ and $T_s$ can be tuned to model different volatile state sizes.

Before the simulation, we developed and explored two simulation processes: (a) ~~to~~ simulate system state with a fine-grained time step, and (b) ~~to~~ sort energy source conditions into a distribution in time lengths and process the distribution. Process (b) shows a MAPE of only 0.892% compared to Process (a), ~~but reduces~~ simulation time significantly (e.g. from several hours to several seconds in a one-year test). Hence, we use Process (b) in the following tests.

## VI. EXPLORATION

This section first shows an exploration of how to improve forward progress by sizing energy storage with respect to supply current and volatile state size (Section VI-A), and then demonstrates the sizing process of energy storage in real-world energy source conditions (Section VI-B) with a trade-off in forward progress, capacitor volume, and recharging time (Section VI-C).

### A. Sizing Energy Storage to Improve Forward Progress

*1) Impact of Supply Current:* Increasing energy storage capacity improves forward progress by prolonging the period of operating cycles and reducing the number of restore and save operations compared to the minimum energy storage. The relationship of forward progress and energy storage capacity is plotted given a range of constant current supply in Fig. 5. Forward progress increases as energy storage capacity increases beyond the minimum level (6.2 µF in this case). However, this improvement is offset by increased capacitor leakage, which leads to an optimal storage capacity.

When capacity is less than the minimum (in Fig. 5, the area on the left of the dashed line), the execution may still progress given that the current supply keeps providing energy during execution. However, if the restore or save operation cannot be completed even with the energy income during execution, the forward progress directly falls to zero as the volatile state cannot be preserved completely. There is a 'steep downfall' because the implemented control algorithm enters the low-power mode with volatile state retained after a save operation, and hence, as long as the supply voltage recovers to the restore threshold without a power failure (which is achieved by the constant current supply), the energy budget used for restoring state at first is then used for effective execution in the following operating cycles.

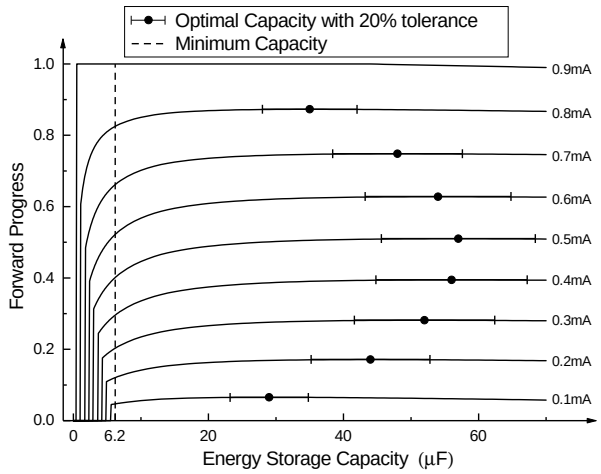


Fig. 5. Forward progress against energy storage capacity given different levels of constant supply current.

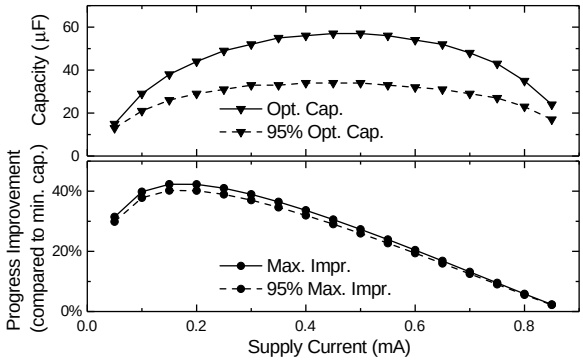


Fig. 6. Maximum forward progress improvement by sizing energy storage given a spectrum of supply current, with the corresponding optimal and sub-optimal (95% of maximum improvement) capacitance.

As a further illustration shown in Fig. 6, the maximum forward progress improvement, compared to using the minimum energy storage, can achieve up to 42.3% with regard to a range of supply current. Typically, capacitors in manufacture has $\pm$20% tolerance of capacitance. This effect of capacitance variations on forward progress is also plotted in Fig. 5, where it is shown to be trivial (<0.7% of the optimal values). Correspondingly, the optimal energy storage capacity is also plotted against supply current. It may not be preferable to optimise the energy storage capacitor with the sole goal of maximising forward progress because other concerns exist in increasing capacity, e.g. recharging time and dimensions (latter explained in Section VI-C). As we observe that the progress change is trivial around the optimal storage capacity, we also plot in Fig. 6 the storage capacity which achieves 95% of the maximum improvement, with a significant reduction of capacity (e.g. from 57 μF to 34 μF at 0.5 mA supply).

*2) Impact of Volatile State Size:* The size of volatile state differs across different applications due to their different amounts of RAM usage, and hence, incurs application-specific time overheads for restore and save operations. Although such overheads are profiled for one application in Section V, the model can be used to explore other applications with

TABLE IV
LINEAR SCALING RANGE OF VOLATILE STATE SIZE AND RESTORE/SAVE TIME OVERHEADS

| State Size (Registers + SRAM) | Restore Time | Save Time |
|---|---|---|
| 64B + 160B (lower bound) | 232 μs | 208 μs |
| 64B + 2048B (upper bound) | 2.298 ms | 2.274 ms |

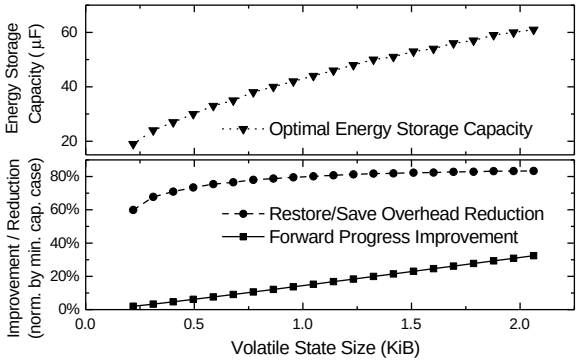


Fig. 7. Impact of RAM usage (linear to restore/save overhead) on sizing energy storage with 0.4 mA current supply.

various volatile state sizes. We modelled the volatile state size variations by linearly scaling restore and save time overheads, as the time overheads of restore and save operations are linear to the size of volatile state [18]. We measured time overheads of restore and save operations in the minimum case (64B register data and a 160B stack) and the maximum case (64B register data and 2048B full RAM) respectively, with the results shown in TABLE IV.

An example of this exploration on volatile state size is plotted in Fig. 7 with 0.4 mA supply current. The forward progress improvement that can be gained from sizing energy storage increases with the volatile state size, and the optimal storage capacity grows accordingly. Such benefit becomes insignificant when the volatile state size is small because the restore and save overheads are already negligible. For example, when the workload uses the least volatile state (the left end point in Fig. 7), the maximum progress improvement is only 2% although the restore and save overheads are reduced by 60%.

### *B. Optimising Energy Storage in Deploying EHTC Devices under Real-World Energy Source Conditions*

In the practical deployment of EHTC devices, ambient energy source conditions change over time and locations. The energy harvester and energy storage should be configured accordingly to achieve desired forward progress across various energy source conditions. Four light source datasets across different environments are used in the following tests. We demonstrate the sizing process under the four datasets for a PV-based EHTC device.

Three levels of minimum forward progress (target $\alpha_{exe}$) are assumed to be 0.1, 0.2, and 0.3. To explore the energy harvester size needed for the above forward progress targets, we plot the forward progress against energy harvester size and

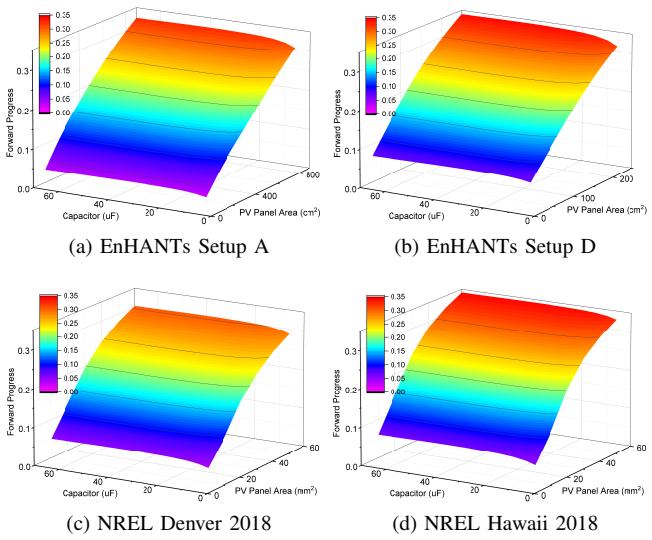


(a) EnHANTs Setup A (b) EnHANTs Setup D

(c) NREL Denver 2018 (d) NREL Hawaii 2018

Fig. 8. Forward progress against energy harvester size and energy storage capacity in real-world energy source conditions.

energy storage capacity in Fig. 8. The model is able to explore the relationship between the allocated harvester size and the expected progress. The energy harvester size to achieve desired forward progress may span over orders of magnitude given different energy source conditions (from $mm^2$ for outdoor to $cm^2$ for indoor sources).

TABLE V lists the PV panel area to achieve the target $\alpha_{exe}$ with minimum energy storage capacity, the optimal capacity with the forward progress improvement, and the alternative (decreased) PV panel area with the optimal capacity. A takeaway from this result is that optimising energy storage can either improve forward progress or reduce energy harvester size. In order to improve forward progress with less dimensional overheads, it is efficient to increase energy harvester size given strong energy sources (e.g. cost tens of $mm^2$ in outdoor source 1 and 2); however, it is economic to optimise energy storage capacity given weak energy sources (e.g. save tens of $cm^2$ in indoor source 1 and 2).

TABLE V
ENERGY HARVESTER SIZE TO ACHIEVE TARGET $\alpha_{exe}$ WITH OPTIMAL ENERGY STORAGE CAPACITY TO IMPROVE FORWARD PROGRESS OR REDUCE ENERGY HARVESTER SIZE

| Target $\alpha_{exe}$ | PV Panel Area w/ Min. C | Optimal C for $\alpha_{exe}$ / Impr. of $\alpha_{exe}$ | Alternative Panel Area / C |
|---|---|---|---|
| Indoor Source 1, EnHANTs Setup A | | | |
| 0.1 | 277 $cm^2$ | 44 µF / +22.3% | 226 $cm^2$ / 42 µF |
| 0.2 | 570 $cm^2$ | 48 µF / +15.2% | 482 $cm^2$ / 48 µF |
| 0.3 | 891 $cm^2$ | 42 µF / + 7.5% | 802 $cm^2$ / 44 µF |
| Indoor Source 2, EnHANTs Setup D | | | |
| 0.1 | 59 $cm^2$ | 37 µF / +16.9% | 49 $cm^2$ / 34 µF |
| 0.2 | 137 $cm^2$ | 45 µF / +14.3% | 116 $cm^2$ / 43 µF |
| 0.3 | 235 $cm^2$ | 47 µF / + 9.6% | 203 $cm^2$ / 47 µF |
| Outdoor Source 1, NREL Denver 2018 | | | |
| 0.1 | 21 $mm^2$ | 46 µF / +26.3% | 18 $mm^2$ / 45 µF |
| 0.2 | 35 $mm^2$ | 45 µF / +11.6% | 31 $mm^2$ / 45 µF |
| 0.3 | 66 $mm^2$ | 45 µF / + 5.5% | 58 $mm^2$ / 45 µF |
| Outdoor Source 2, NREL Hawaii 2018 | | | |
| 0.1 | 19 $mm^2$ | 48 µF / +28.7% | 16 $mm^2$ / 46 µF |
| 0.2 | 30 $mm^2$ | 45 µF / +12.9% | 27 $mm^2$ / 46 µF |
| 0.3 | 50 $mm^2$ | 45 µF / + 5.8% | 45 $mm^2$ / 45 µF |

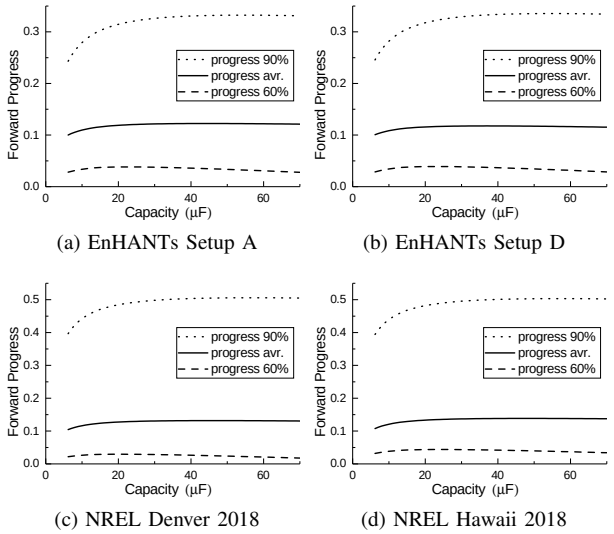


(a) EnHANTs Setup A (b) EnHANTs Setup D

(c) NREL Denver 2018 (d) NREL Hawaii 2018

Fig. 9. Percentiles of forward progress by sizing energy storage with target $\alpha_{exe}$ = 0.1 and the corresponding PV panel area listed in TABLE V. The percentiles start from 60% as the system is off for around 55% of time due to insufficient energy source.

### C. Trading off Forward Progress, Dimensions, and Recharging Time

Although increasing the storage capacity improves forward progress, larger capacitance may impact both dimensions and recharging time. We evaluate the overheads of increased capacitor dimensions and recharging time, and then trade off them with forward progress using a cost function to suggest an optimal capacitor size.

*1) Dimensions:* The overhead of capacitor dimensions is evaluated by looking into various off-the-shelf tantalum capacitors. We narrow down the range of sample capacitors within a set of characteristics: low-profile, 10V rated voltage, and Surface Mount Device (SMD) package, and select six series of capacitors. The volume and capacitance of these capacitors are plotted in Fig. 10 according to their datasheets [38]–[43]. The closest available capacitance that ensures the minimum storage is 6.8 µF, whereas the closest available capacitance to achieve the optimal capacitance in TABLE V are 33 µF or 47 µF (depending on different energy conditions and harvester sizes). The minimum volume for these three capacitance are 2.75 $mm^3$, 2.75 $mm^3$, and 5.12 $mm^3$, which means using the optimal capacitance instead of the minimum one may not incur dimensional overhead (for 33 µF). For 47 µF, the absolute volume (5.12 $mm^3$) is still insignificant compared to the device as a whole, e.g. an MSP430FR6989 MCU chip alone occupies 14 × 14 × 1.4 $mm^3$ (274.4 $mm^3$). We also evaluated the regressed volume of the above three capacitance values, which are 8.1 $mm^3$, 23.8 $mm^3$, 30.4 $mm^3$ respectively. Again, such is still insignificant compared to the device as a whole.

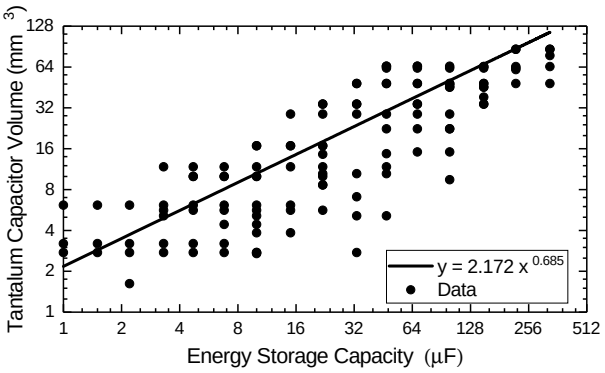


Fig. 10. Tantalum capacitor volume against capacitance [38]–[43].

*2) Recharging Time:* A transient node cannot immediately process an event during the recharging period between two active periods. However, this recharging delay might be crucial to some event-capturing applications.

Technically, the actual recharging time between two active periods depends on capacitance, the start and end voltage of recharging, and the current income and consumption. While the end voltage (restore voltage) and current consumption can be set or predicted, the start voltage and current flows vary with energy source conditions. Instead of evaluating the recharging time in complex conditions, we use the time between two successive execution intervals in the Switch mode as the metric of recharging time or recharging ability.

Using Equation (4) and (6), we can obtain this recharging period between two successive execution intervals in the Switch mode as:

$$\begin{aligned} T_{recharge} &= T_{period} - T_{exe} \\ &= \frac{C(V_r - V_s) + T_s(I_{in} - I_s)}{I_{in} - I_{sleep}} + T_r \end{aligned} \tag{14}$$

*3) Trade-offs:* Fig. 11.

Tested with the cost function configured as:

$$f = \frac{\alpha_{exe}}{0.2} - (\frac{v_{cap}}{200})^2 - T^2_{recharge} \tag{15}$$

with $v_{cap}$ in mm$^3$ and $T_{recharge}$ in second.

## VII. Model Validation

This section shows the comparison between the experimental and modelled forward progress to evaluate the accuracy of the proposed reactive transient computing model. Also, the forward progress with a properly-sized capacitor is compared to that with a minimum one, an on-board one, and an ideal case given a range of supply current.

### A. Experiment Setup

With the identical platform properties and workload settings in simulation setup, we used the TI MSP430FR6989 development board as the test platform. The on-board capacitance is measured to be 10.0 µF. This is the minimum capacitance that can be experimented on the platform. Additional capacitors were added to provide extra energy storage. The leakage current of these capacitors are less than 10 nA at 3 V, which is negligible compared to the current consumption of the platform (µA current draw), and hence, we omit the leakage of capacitors in the following experiment and model comparison.

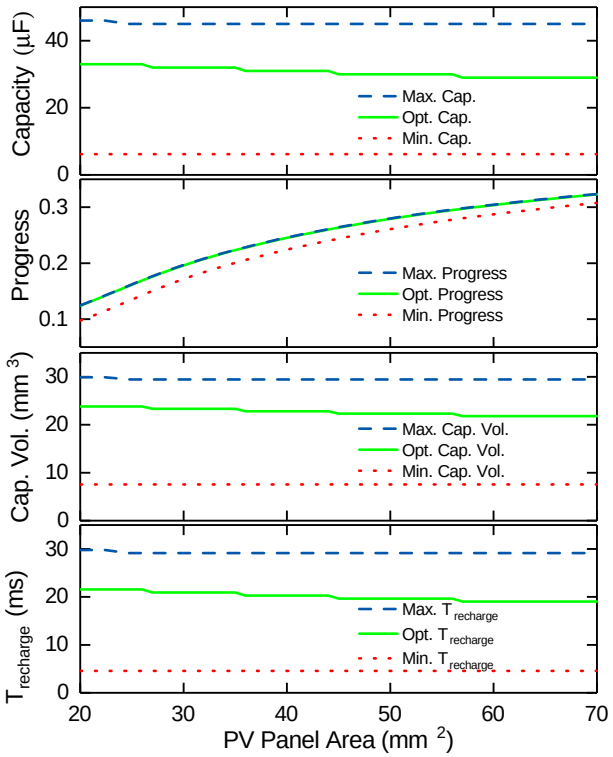


Fig. 11. The sizing process trades off forward progress, capacitor volume, and recharging time. The results are plotted against a range of PV panel area, given Denver 2018 energy source dataset.

In this practical experiment, the task completion rate (i.e. tasks completed per second) is used as the metric of forward progress rather than the effective execution time ratio. To gain the task completion rate from the model, we multiply the execution time ratio generated from our model by the completion rate when the device is executing constantly, since the task completion rate is linear to the effective execution time.

### B. Validation

*1) Model Accuracy:* To validate the accuracy of our model, we powered the device with a range of current supply to operate the device in the Switch mode (0.1 to 0.8 mA), and repeated the tests with three energy storage capacities: 1) on-board 10.0 µF capacitance only; 2) 21.5 µF measured in total (11.5 µF added); 3) 43.0 µF measured in total (33.0 µF added). We compared the actual program completion speed with the one that our model generated. As shown in Fig. 12, the model generated output matches closely with the experimental results with only 0.5% MAPE. Hence, the model is able to accurately estimate forward progress for design exploration.

*2) Forward Progress Optimisation:* Properly sizing energy storage benefits forward progress. We compared the tested completion speed with 10 µF and 43 µF to a theoretical

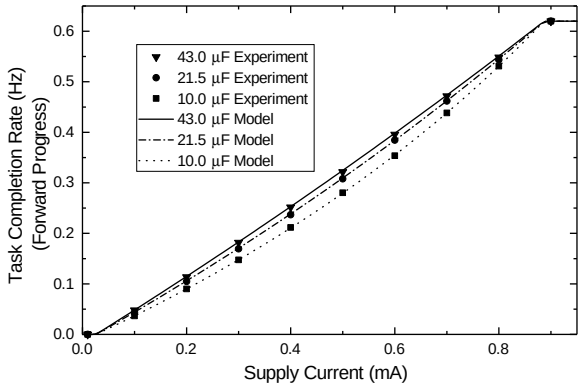


Fig. 12. Model validation by comparing the experimented and modelled task completion rates (forward progress) with different capacitance and supply current.

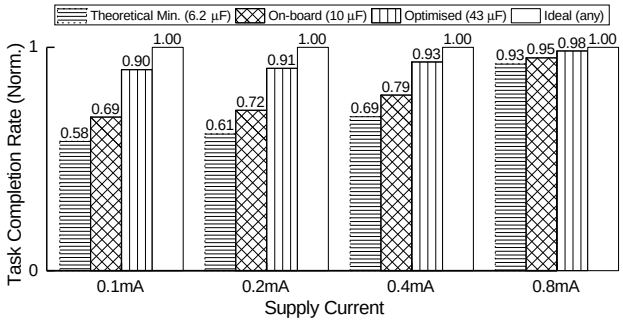


Fig. 13. Experimental comparison of task completion rates (forward progress) among different energy storage capacity.

minimum capacity case (model generated) and an ideal case. The ideal case does not incur overheads of restoring and saving, only switching between the sleep mode and the active mode (mentioned in Section III-B). As shown in Fig. 13, a reasonably sized energy storage capacity (43μF) improves up to 55.2% and 30.4% more progress compared to the theoretical minimum capacitance and the platform on-board capacitance respectively, and also maintain at least 90% of the ideal forward progress. The forward progress improvement by sizing energy storage is significant when supply is weak and relatively insignificant when supply is strong.

## VIII. Conclusion

We proposed a model of reactive transient computing to estimate forward progress. Using this model, we explored the sizing effect of energy storage on forward progress in reactive transient computing with respect to supply current and volatile state size. We proposed a process of sizing energy storage in deploying EHTC devices, which trades off forward progress, capacitor dimensions, and recharging time. We integrated the model in a PV-based EHTC device framework to demonstrate the sizing process, where results show that a reasonbly energy storage capacity, rather than a minimum one, can improve 5.5-28.7% mean forward progress, while balance capacitor volume and recharging delay, given four different one-year real-world energy source datasets. In experiments, we validated the reactive transient computing model with 0.5% MAPE, and showed that a reasonbly sized 43 μF capacitor improves forward progress by up to 55.2% and 30.4% compared to a theoretical minimum 6.2 μF one and an on-board 10 μF one across various levels of supply current.

## Appendix
## Calculation Breakdown of Differential Analysis

Haven't decided whether to attach this or not.

## References

[1] L. Mainetti, L. Patrono, and A. Vilei, "Evolution of wireless sensor networks towards the internet of things: A survey," in *SoftCOM 2011, 19th International Conference on Software, Telecommunications and Computer Networks*, Sep. 2011, pp. 1–6.

[2] O. Hahm, E. Baccelli, H. Petersen, and N. Tsiftes, "Operating systems for low-end devices in the internet of things: A survey," *IEEE Internet of Things Journal*, vol. 3, no. 5, pp. 720–734, Oct 2016.

[3] T. Adegbija, A. Rogacs, C. Patel, and A. Gordon-Ross, "Microprocessor optimizations for the internet of things: A survey," *IEEE Transactions on Computer-Aided Design of Integrated Circuits and Systems*, vol. 37, no. 1, pp. 7–20, Jan 2018.

[4] W. Shi, J. Cao, Q. Zhang, Y. Li, and L. Xu, "Edge computing: Vision and challenges," *IEEE Internet of Things Journal*, vol. 3, no. 5, pp. 637–646, Oct 2016.

[5] Sravanthi Chalasani and J. M. Conrad, "A survey of energy harvesting sources for embedded systems," in *IEEE SoutheastCon 2008*, April 2008, pp. 442–447.

[6] S. Sudevalayam and P. Kulkarni, "Energy harvesting sensor nodes: Survey and implications," *IEEE Communications Surveys Tutorials*, vol. 13, no. 3, pp. 443–461, Third 2011.

[7] A. Kansal, J. Hsu, S. Zahedi, and M. B. Srivastava, "Power management in energy harvesting sensor networks," *ACM Trans. Embed. Comput. Syst.*, vol. 6, no. 4, Sep. 2007. [Online]. Available: http://doi.acm.org/10.1145/1274858.1274870

[8] B. Buchli, F. Sutton, J. Beutel, and L. Thiele, "Dynamic power management for long-term energy neutral operation of solar energy harvesting systems," in *Proceedings of the 12th ACM Conference on Embedded Network Sensor Systems*, ser. SenSys '14. New York, NY, USA: ACM, 2014, pp. 31–45. [Online]. Available: http://doi.acm.org/10.1145/2668332.2668333

[9] P. Wägemann, T. Distler, H. Janker, P. Raffeck, V. Sieh, and W. SchröDer-Preikschat, "Operating energy-neutral real-time systems," *ACM Trans. Embed. Comput. Syst.*, vol. 17, no. 1, pp. 11:1–11:25, Aug. 2017. [Online]. Available: http://doi.acm.org/10.1145/3078631

[10] X. Jiang, J. Polastre, and D. Culler, "Perpetual environmentally powered sensor networks," in *Proceedings of the 4th International Symposium on Information Processing in Sensor Networks*, ser. IPSN '05. Piscataway, NJ, USA: IEEE Press, 2005. [Online]. Available: http://dl.acm.org/citation.cfm?id=1147685.1147765

[11] F. Simjee and P. H. Chou, "Everlast: Long-life, supercapacitor-operated wireless sensor node," in *Proceedings of the 2006 International Symposium on Low Power Electronics and Design*, ser. ISLPED '06. New York, NY, USA: ACM, 2006, pp. 197–202. [Online]. Available: http://doi.acm.org/10.1145/1165573.1165619

[12] B. Ransford, J. Sorber, and K. Fu, "Mementos: System support for long-running computation on RFID-scale devices," in *Proceedings of the Sixteenth International Conference on Architectural Support for Programming Languages and Operating Systems*, ser. ASPLOS XVI. New York, NY, USA: ACM, 2011, pp. 159–170. [Online]. Available: http://doi.acm.org/10.1145/1950365.1950386

[13] H. Jayakumar, A. Raha, and V. Raghunathan, "QUICKRECALL: A low overhead HW/SW approach for enabling computations across power cycles in transiently powered computers," in *2014 27th International Conference on VLSI Design and 2014 13th International Conference on Embedded Systems*, Jan 2014, pp. 330–335.

[14] D. Balsamo, A. S. Weddell, G. V. Merrett, B. M. Al-Hashimi, D. Brunelli, and L. Benini, "Hibernus: Sustaining computation during intermittent supply for energy-harvesting systems," *IEEE Embedded Systems Letters*, vol. 7, no. 1, pp. 15–18, March 2015.

[15] B. Lucia and B. Ransford, "A simpler, safer programming and execution model for intermittent systems," in *Proceedings of the 36th ACM SIGPLAN Conference on Programming Language Design and Implementation*, ser. PLDI '15. New York, NY, USA: ACM, 2015, pp. 575–585. [Online]. Available: http://doi.acm.org/10.1145/2737924.2737978

[16] Y. Wang, Y. Liu, S. Li, D. Zhang, B. Zhao, M. Chiang, Y. Yan, B. Sai, and H. Yang, "A 3us wake-up time nonvolatile processor based on ferroelectric flip-flops," in *2012 Proceedings of the ESSCIRC (ESSCIRC)*, Sep. 2012, pp. 149–152.

[17] J. V. D. Woude and M. Hicks, "Intermittent computation without hardware support or programmer intervention," in *12th USENIX Symposium on Operating Systems Design and Implementation (OSDI 16)*. Savannah, GA: USENIX Association, Nov. 2016, pp. 17–32. [Online]. Available: https://www.usenix.org/conference/osdi16/technical-sessions/presentation/vanderwoude

[18] S. T. Sliper, D. Balsamo, N. Nikoleris, W. Wang, A. S. Weddell, and G. V. Merrett, "Efficient state retention through paged memory management for reactive transient computing," in *Proceedings of the 56th Annual Design Automation Conference 2019*, ser. DAC '19. New York, NY, USA: ACM, 2019, pp. 26:1–26:6. [Online]. Available: http://doi.acm.org/10.1145/3316781.3317812

[19] K. Ma, X. Li, K. Swaminathan, Y. Zheng, S. Li, Y. Liu, Y. Xie, J. J. Sampson, and V. Narayanan, "Nonvolatile processor architectures: Efficient, reliable progress with unstable power," *IEEE Micro*, vol. 36, no. 3, pp. 72–83, May 2016.

[20] K. Ma, Y. Zheng, S. Li, K. Swaminathan, X. Li, Y. Liu, J. Sampson, Y. Xie, and V. Narayanan, "Architecture exploration for ambient energy harvesting nonvolatile processors," in *2015 IEEE 21st International Symposium on High Performance Computer Architecture (HPCA)*, Feb 2015, pp. 526–537.

[21] D. Balsamo, A. S. Weddell, A. Das, A. R. Arreola, D. Brunelli, B. M. Al-Hashimi, G. V. Merrett, and L. Benini, "Hibernus++: A self-calibrating and adaptive system for transiently-powered embedded devices," *IEEE Transactions on Computer-Aided Design of Integrated Circuits and Systems*, vol. 35, no. 12, pp. 1968–1980, 2016.

[22] D. Balsamo, A. Das, A. S. Weddell, D. Brunelli, B. M. Al-Hashimi, G. V. Merrett, and L. Benini, "Graceful performance modulation for power-neutral transient computing systems," *IEEE Transactions on Computer-Aided Design of Integrated Circuits and Systems*, vol. 35, no. 5, pp. 738–749, May 2016.

[23] J. Hester, L. Sitanayah, and J. Sorber, "Tragedy of the coulombs: Federating energy storage for tiny, intermittently-powered sensors," in *Proceedings of the 13th ACM Conference on Embedded Networked Sensor Systems*, ser. SenSys '15. New York, NY, USA: Association for Computing Machinery, 2015, p. 5–16. [Online]. Available: https://doi.org/10.1145/2809695.2809707

[24] D. Balsamo, B. J. Fletcher, A. S. Weddell, G. Karatziolas, B. M. Al-Hashimi, and G. V. Merrett, "Momentum: Power-neutral performance scaling with intrinsic mppt for energy harvesting computing systems," *ACM Trans. Embed. Comput. Syst.*, vol. 17, no. 6, Jan. 2019. [Online]. Available: https://doi.org/10.1145/3281300

[25] K. Maeng and B. Lucia, "Adaptive dynamic checkpointing for safe efficient intermittent computing," in *13th USENIX Symposium on Operating Systems Design and Implementation (OSDI 18)*. Carlsbad, CA: USENIX Association, Oct. 2018, pp. 129–144. [Online]. Available: https://www.usenix.org/conference/osdi18/presentation/maeng

[26] K. Maeng, A. Colin, and B. Lucia, "Alpaca: Intermittent execution without checkpoints," *Proc. ACM Program. Lang.*, vol. 1, no. OOPSLA, pp. 96:1–96:30, Oct. 2017. [Online]. Available: http://doi.acm.org/10.1145/3133920

[27] K. Maeng and B. Lucia, "Supporting peripherals in intermittent systems with just-in-time checkpoints," in *Proceedings of the 40th ACM SIGPLAN Conference on Programming Language Design and Implementation*, ser. PLDI 2019. New York, NY, USA: ACM, 2019, pp. 1101–1116. [Online]. Available: http://doi.acm.org/10.1145/3314221.3314613

[28] F. Su, Y. Liu, X. Sheng, H. G. Lee, N. Chang, and H. Yang, "A task failure rate aware dual-channel solar power system for nonvolatile sensor nodes," *ACM Trans. Embed. Comput. Syst.*, vol. 18, no. 4, pp. 33:1–33:21, Jul. 2019. [Online]. Available: http://doi.acm.org/10.1145/3320270

[29] J. San Miguel, K. Ganesan, M. Badr, and N. E. Jerger, "The EH model: Analytical exploration of energy-harvesting architectures," *IEEE Computer Architecture Letters*, vol. 17, no. 1, pp. 76–79, Jan 2018.

[30] J. San Miguel, K. Ganesan, M. Badr, C. Xia, R. Li, H. Hsiao, and N. Enright Jerger, "The EH model: Early design space exploration of intermittent processor architectures," in *2018 51st Annual IEEE/ACM International Symposium on Microarchitecture (MICRO)*, Oct 2018, pp. 600–612.

[31] N. Jackson, J. Adkins, and P. Dutta, "Capacity over capacitance for reliable energy harvesting sensors," in *Proceedings of the 18th International Conference on Information Processing in Sensor Networks*, ser. IPSN '19. New York, NY, USA: ACM, 2019, pp. 193–204. [Online]. Available: http://doi.acm.org/10.1145/3302506.3310400

[32] A. Andreas and T. Stoffel, "NREL solar radiation research laboratory (SRRL): Baseline measurement system (bms); golden, colorado (data)," *NREL Report NO.DA-5500-56488*, 1981.

[33] M. Gorlatova, A. Wallwater, and G. Zussman, "Networking low-power energy harvesting devices: Measurements and algorithms," *IEEE Transactions on Mobile Computing*, vol. 12, no. 9, pp. 1853–1865, Sep. 2013.

[34] S. Vergura, "A complete and simplified datasheet-based model of PV cells in variable environmental conditions for circuit simulation," *Energies*, vol. 9, no. 5, 2016. [Online]. Available: http://www.mdpi.com/1996-1073/9/5/326

[35] Panasonic, "Amorton amorphous silicon solar cells."

[36] Nichicon, "UPW aluminum electrolytic capacitors," http://www.nichicon.co.jp/english/products/pdfs/e-upw.pdf, last accessed: 15 May, 2019.

[37] R. Faltus, "Low leakage current aspect of designing with tantalum and niobium oxide capacitors," https://www.avx.com/docs/techinfo/Low_Leakage_Current_Aspect_Designing_Tantalum_Niobium_Oxide_Capacitors.pdf, last accessed: 28 Jan, 2019.

[38] AVX, "AVX TAJ low profile series tantalum capacitors," http://datasheets.avx.com/TAJ_LOW_PROFILE.pdf, last accessed: 2 Dec, 2019.

[39] ——, "AVX TACmicrochip low profile series tantalum capacitors," http://datasheets.avx.com/TAC_LP.pdf, last accessed: 2 Dec, 2019.

[40] ——, "AVX F92 series tantalum capacitors," http://datasheets.avx.com/F92.pdf, last accessed: 2 Dec, 2019.

[41] Vishay, "Vishay 572D series tantalum capacitors," http://www.vishay.com/docs/40064/572d.pdf, last accessed: 2 Dec, 2019.

[42] ——, "Vishay 591D series tantalum capacitors," https://www.vishay.com/docs/40012/591d.pdf, last accessed: 2 Dec, 2019.

[43] ——, "Vishay 592D series tantalum capacitors," http://www.vishay.com/docs/40004/592d.pdf, last accessed: 2 Dec, 2019.